AIAA 98–0585

Dynamic Calibration of a Shear Stress Sensor Using Stokes Layer Excitation

Mark Sheplak, Aravind Padmanabhan,
Martin A. Schmidt, Kenneth S. Breuer

Microsystems Technology Laboratory
Massachusetts Institute of Technology
Cambridge, MA 02139

36th AIAA Aerospace Sciences Meeting
January 12 - 15, 1998
Reno, NV

Mark Sheplak, Aravind Padmanabhan, Martin A. Schmidt, and Kenneth S. Breuer. "Dynamic Calibration of a Shear-Stress Sensor Using Stokes-Layer Excitation", AIAA Journal, Vol. 39, No. 5 (2001), pp. 819-823. , https://doi.org/10.2514/2.1415

Dynamic Calibration of a Shear Stress Sensor Using Stokes Layer Excitation

Mark Sheplak[*], Aravind Padmanabhan[†],
Martin A. Schmidt[‡], Kenneth S. Breuer[§]

Microsystems Technology Laboratory
Massachusetts Institute of Technology
Cambridge, MA 02139

The design and implementation of a novel dynamic calibration technique for shear-stress sensors is presented. This technique utilizes the oscillating wall shear stress generated by a traveling acoustic wave as a known input to the shear-stress sensor. A silicon-micromachined, floating-element shear stress sensor has been dynamically calibrated up to 4 kHz using this method. This data represents the first broad-band, experimental verification of the dynamic response of a shear-stress sensor.

Introduction

The measurement of shear-stress fluctuations in a turbulent boundary layer is of vital importance to the fluid mechanics community, because it provides important information about flow phenomena, including viscous drag, transition to turbulence, and flow separation.[1] To accurately capture the spectrum of the turbulent shear-stress fluctuations, the measurement device must possess a large usable bandwidth and the spatial dimensions of the device must be smaller than the turbulent structures to be measured. The spatial length scales of interest are typically on the order of a hundred microns and the required bandwidth is in excess of 10 kHz.[2] The stringent spatial and temporal resolution requirements naturally point to a microfabricated transducer as a means of achieving this level of performance, and a number of researchers have demonstrated device designs aimed at meeting this goal [2-13]. Existing wall shear stress sensors can be grouped by measurement method into two distinct classes, direct techniques such as floating element type devices)[2,3,5,6,9–11] or indirect techniques such as hot wires or hot films.[4,6–8,12,13]

For turbulence measurements, it is desirable that the shear-stress sensor possess an optimally-flat, unity-gain, minimum-phase frequency response function. Such characteristics are necessary to minimize the uncertainty in correlation and spectral analysis data. The actual dynamic response, however, will be band-limited because of the inherent compliance, inertance, and dissipation of the measurement system. For direct measurement techniques, either the fluidic damping or the resonant frequency associated with the floating element structure defines the usable bandwidth. In thermal systems, the bandwidth is usually limited by the thermal inertia of the sensing element. In addition, the dynamic response of thermal sensors is complicated by the frequency-dependent heat conduction into the supporting structure (*i.e.,* substrate[14,15] or membrane[7] for hot films and prongs for hot wires[8,16]) which creates a low-frequency roll-off in the gain factor of the frequency response function, as well as a corresponding frequency-dependent phase lag. The difficulties associated with the modeling of time-resolved microscale phenomena, fluidic damping for floating elements and the conjugated heat-transfer problem for thermal sensors, precludes the accurate prediction of the frequency response function for both classes of shear-stress sensors. Therefore, it is necessary to characterize the frequency response function of the sensor via *in-situ* dynamic calibration. Unfortunately, obtaining a known broadband shear-stress input for direct dynamic calibration is difficult in practice. Recently, a technique has been reported which calibrates shear-stress sensors using acoustically generated Stokes waves at various frequencies within a flat-plate boundary layer.[17] The Stokes wave is generated in the wind tunnel test section at a given frequency within a pre-determined range via an array of nine speakers. The shear stress on the surface is calculated using a hot-wire velocity measurement at the same streamwise location as the surface-mounted sensor. This method has been used over a frequency range from 50 Hz to 3.0 kHz. This technique is very useful for absolute calibrations, but it requires a dedicated wind-tunnel facility outfitted with a speaker array and is ultimately band-limited due to measurement spatial resolution within the Stokes layer velocity profile (*i.e.,* $\delta(f) \approx 6.5(\nu/2\pi f)^{1/2}$,[18] $\delta(3\ kHz) \approx 183\ \mu m$).

This paper presents the development of a self-contained acoustic plane wave generator which pro-

[*] Postdoctoral Associate, Member AIAA.
[†] Graduate Student.
[‡] Associate Professor.
[§] Associate Professor, Department of Aeronautics and Astronautics. Member AIAA.

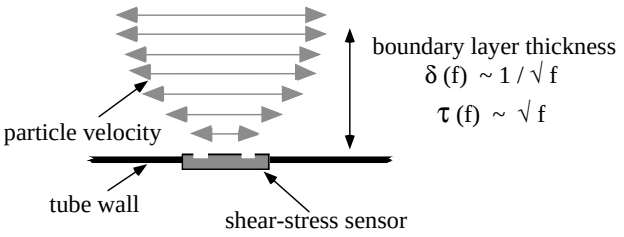

Fig. 1 Schematic of acoustic-wave particle motion near the wall.

vides a known sinusoidal shear input to a shear-stress sensor. In this calibration technique, the sinusoidal shear stress is inferred from the cylindrical Stokes layer solution for a plane acoustic wave traveling in a circular duct. The theoretical aspects of this technique are discussed and representative calibration results from a floating-element sensor presented.

Background

The dynamic response of a general shear-stress sensor system is band-limited because of the various modes of energy storage and dissipation inherent in the system. Assuming that the shear-stress sensor can be modeled as a linear, time-invariant system over a range of shear stress, dynamic calibration is possible, provided that a known sinusoidal shear input can be produced.[19,20] In this section, the theoretical basis for dynamically calibrating linear shear-stress sensors via Stokes layer excitation in a cylindrical duct is presented.

Stokes Layer Excitation

The basic principle of this technique relies on the fact that the particle velocity of acoustic waves must equal zero at the duct wall. The consequence of the no-slip boundary condition is the generation of a frequency-dependent boundary layer ($\delta(f)$) and wall-shear stress ($\tau(f)$)[18] (see Figure 1). For the case of purely-traveling plane waves in a duct with no mean flow, the linearized perturbation equation for the compressible momentum conservation law in the axial direction reduces to the classic problem of a duct-flow driven by an oscillating pressure gradient. The solution to this problem indicates that the magnitude of the shear-stress is directly proportional to the product of the pressure magnitude and the square-root of the excitation frequency.[18]

The problem of duct-flow driven by an oscillating pressure gradient was originally investigated experimentally by Richardson and Tyler (1929)[21] then solved analytically by Sexl (1930).[22] This problem is also discussed in White (1974).[18] Assuming an axial velocity, $u(r,t)$, where r is the radial coordinate, the differential form of the momentum conservation law in the axial direction, z is

$$\frac{\partial u}{\partial t} = -\frac{1}{\rho}\frac{\partial p}{\partial z}e^{\jmath 2\pi f t} + \nu\frac{\partial^2 u}{\partial r^2} + \nu\frac{1}{r}\frac{\partial u}{\partial r}, \qquad (1)$$

where, ρ is the density, ν is the kinematic viscosity, and $\frac{\partial p}{\partial z}$ is the magnitude of the oscillating pressure gradient. Assuming a harmonic solution, the boundary conditions to the problem consist of a finite velocity at the tube center and the no-slip condition at the tube wall, $r = R$,

$$u(0,t) < \infty \qquad and \qquad u(R,t) = 0. \qquad (2)$$

The solution of Equation (1) for the particle velocity, u, is

$$u(r,t) = -\frac{e^{\jmath 2\pi f t}}{\jmath 2\pi f \rho}\frac{\partial p}{\partial z}\left[1 - \frac{I_0\left(r\sqrt{\jmath 2\pi f/\nu}\right)}{I_0\left(R\sqrt{\jmath 2\pi f/\nu}\right)}\right], \qquad (3)$$

where, I_0 is the zeroth-order, modified Bessel function[23] and μ is the fluid viscosity. The corresponding wall shear stress induced by the oscillating pressure gradient is

$$\tau(2\pi f,t) = \frac{e^{\jmath 2\pi f t}}{\jmath 2\pi f}\frac{\partial p}{\partial z}\sqrt{\jmath\rho 2\pi f\mu}\frac{I_1\left(R\sqrt{\jmath 2\pi f/\nu}\right)}{I_0\left(R\sqrt{\jmath 2\pi f/\nu}\right)}. \qquad (4)$$

If the oscillating pressure gradient is driven by a plane, purely-traveling (in positive z-direction only), acoustic wave,

$$p = p' e^{\jmath(2\pi f t - kz)}, \qquad (5)$$

then the pressure gradient can be expressed as

$$e^{\jmath 2\pi f t}\frac{\partial p}{\partial z} = \frac{-\jmath 2\pi f}{c}p' e^{\jmath(2\pi f t - kz)}, \qquad (6)$$

where, p' is the magnitude of the pressure fluctuation, c is the speed of sound, and k is the axial wave number, $k = 2\pi f/c$. Combining Equations (3), (4), and (6) results in the particle velocity and shear stress generated by a purely-traveling acoustic wave in a circular duct,

$$u(r,t) = \frac{p' e^{\jmath(2\pi f t - kz)}}{\rho c}\left[1 - \frac{I_0\left(r\sqrt{\jmath 2\pi f/\nu}\right)}{I_0\left(R\sqrt{\jmath 2\pi f/\nu}\right)}\right] \qquad (7)$$

and

$$\tau(z,t) = -\frac{p' e^{\jmath(2\pi f t - kz)}\sqrt{\jmath\rho 2\pi f\mu}}{c}\frac{I_1\left(R\sqrt{\jmath 2\pi f/\nu}\right)}{I_0\left(R\sqrt{\jmath 2\pi f/\nu}\right)}. \qquad (8)$$

Equation (8) indicates that the magnitude of the oscillating shear-stress is directly proportional to the product of the acoustic pressure magnitude and the square-root of the excitation frequency.

The validity of this solution will breakdown at higher frequencies, where the assumption of plane-wave propagation is no longer valid. In addition to the plane-wave, propagating in axial direction possessing uniform transverse wavefronts, there are higher-order wave modes which reflect back and forth from the duct walls (see, for example,[24]). Therefore, the frequency bandwidth over which the above solution is valid is dependent on the acoustic waveguide characteristics of the tube.

Plane Wave Propagation in a Tube

The propagation of higher-order modes in a cylindrical duct with zero mean flow is governed by the wave equation for simple harmonic waves (see, for example,[24]),

$$\nabla^2 p' + \left(\frac{2\pi f}{c}\right)^2 p' = 0. \tag{9}$$

For a circular duct of radius R, the eigenfunctions in cylindrical coordinates are

$$p(r,\phi,z,t) = p' e^{\jmath(2\pi f t - k_{mn} z)} \cos(m\phi) J_m\left(\frac{\pi q_{mn} r}{R}\right), \tag{10}$$

where, J_m is the Bessel function of order m[23] and $\pi q_{mn}/R$ is the corresponding eigenvalue[1]. If the walls of the tube are assumed to be rigid, the resulting eigenvalue problem is

$$J'_m(\pi q_{mn}) = 0, \tag{11}$$

where, the prime denotes differentiation with respect to the radial coordinate. The (m,n)th mode has m plane modal surfaces that extend radially outward from center axis and n cylindrical nodes that are concentric about the axis. The corresponding wavenumber is

$$k_{mn} = \sqrt{\left(\frac{2\pi f}{c}\right)^2 - \left(\frac{\pi q_{mn}}{R}\right)^2}. \tag{12}$$

When k_{mn} is real, Equation (10) represents traveling waves, axially propagating in the positive z-direction. If k_{mn} is imaginary, then the mode is evanescent, exponentially decaying as it propagates in the positive z-direction. The fundamental mode, (0,0) has a zero characteristic value and is thus a plane wave. The first higher-order mode that becomes propagational (non-evanescent) is the (1,0) mode or first "spinning" mode. Characteristic value associated with (1,0) is $q_{10} = .5861$ and the corresponding frequency is[24]

$$f_{co} = \frac{.2931c}{R}. \tag{13}$$

This value represents the upper limit or cut-off frequency for the validity for Equation (8) in a tube of radius R. For example, the cut-off frequency for a 0.5 m-radius tube is $\approx 200\ Hz$.

Experimental Apparatus

The experimental study was performed in the Fluid Dynamics Research Laboratory at the Massachusetts Institute of Technology. A plane-wave tube capable of generating purely-traveling, plane acoustic waves was designed and fabricated. Two series of tests were conducted, one to characterize the response of the plane-wave tube, the other to demonstrate the Stokes-layer dynamic calibration technique by calibrating a floating-element shear-stress sensor.

[1] For $m \neq 0$, there are actually two eigenfunctions for a given frequency, $\cos(m\phi)$ and $\sin(m\phi)$.[24]

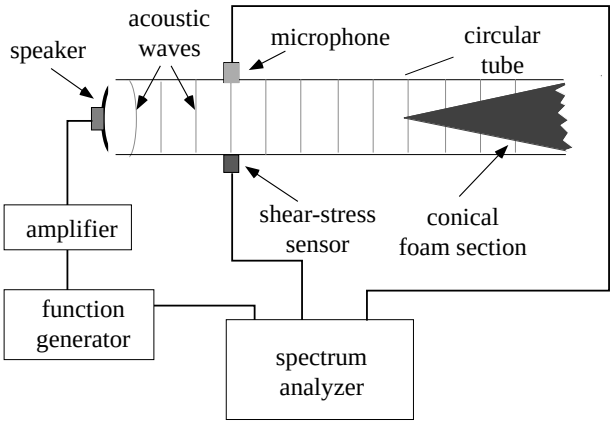

Fig. 2 Schematic of plane-wave tube apparatus used for generating an oscillating shear stress.

Plane Wave Tube

The experimental apparatus used to generate the oscillating Stokes layer, a plane wave tube is shown in Figure 2. The setup includes a 6-foot long, 2″-diameter, 1/8″-thick, circular acrylic tube with a speaker driver (JBL 2446J[27]) attached at one opening and a conical foam section (HyFonic, 80 ppi, Stephenson & Lawyer, Inc.) filling the other end. A Stanford Research Systems SR 830 Lock-In Amplifier provided a sinusoidal input to a Crown DC-300A Series II amplifier which in turn drove the speaker. The conical foam section prevented acoustic reflections by dissipating the incident traveling waves. An 1/8″ microphone (B&K 4138 attached to a B&K 2633 preamplifier) and shear-stress sensor were flush mounted at an axial location 15″ from the speaker driver, 180° opposite one another. The signals from the microphone and shear-stress sensor were recorded by the lock-in amplifier.

As discussed in §2.2, the wave-guide transmission properties of the circular tube determine the propagation characteristics of the acoustic modes. The bandwidth of the calibrator is thus determined by the low-frequency cut-off of the tube, which is defined by the frequency of the first propagating non-planar acoustic mode. The low-frequency cut-off for our tube geometry is $\approx 4\ kHz$ (Equation (13)). The speaker driver will generate higher-order modes, so it is important to locate the shear-stress sensor and microphone a distance greater than $\lambda/6$ ($\lambda = c/f$) downstream of the speaker to ensure measurement of non-evanescent, propagating modes. Proper termination of the plane waves with the foam insert is crucial to prevent wave reflections, which in turn would invalidate the Stokes layer relationship between pressure and shear stress (Equation (8)). Specifically, wave reflections at the tube end will result in a combination of traveling and standing acoustic waves producing nodes and anti-nodes, as well as a phase shift between the particle velocity and the pressure fluctuation.

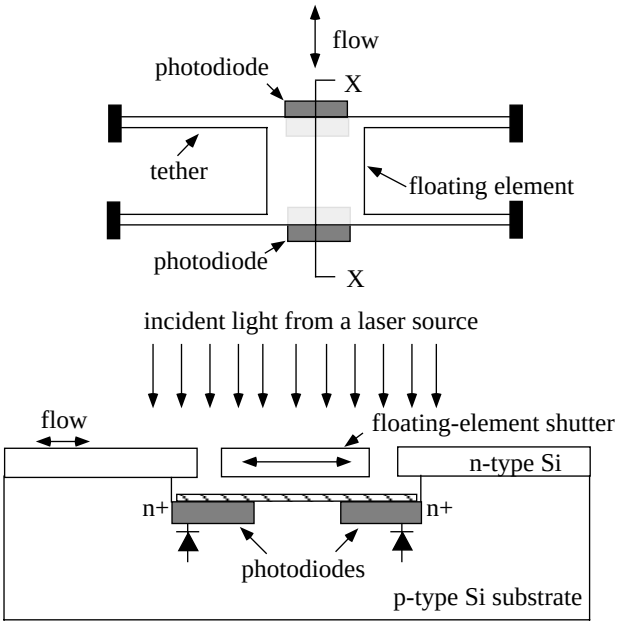

Fig. 3 Schematics of both the top and cross-sectional views of the shear-stress sensor.

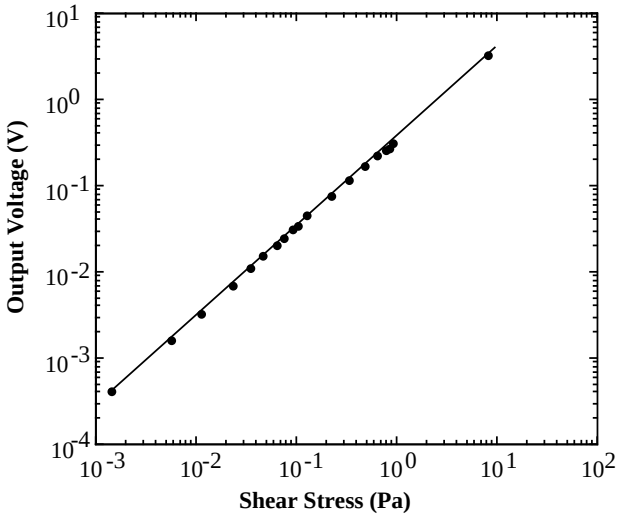

Fig. 4 Static calibration of a $500\ \mu m \times 500\ \mu m \times 7\ \mu m$ **floating-element shear-stress sensor.**

Floating-Element Sensor

We have previously reported the detailed design and fabrication of this sensor.[9,11] The sensor is comprised of a $500\ \mu m \times 500\ \mu m$, square silicon floating element of $7\ \mu m$ thickness which is suspended one micron above the surface of a silicon wafer by four silicon tethers that are $500\ \mu m$ long, $7\ \mu m$ wide, and $7\ \mu m$ thick (see Figure 3). Photodiodes are integrated into the substrate under the floating element at the leading and trailing edge. A modulated light source ($7\ mW$, $670\ nm$ laser diode) illuminates the element from above such that a differential photocurrent is produced which is directly proportional to the lateral displacement of the element and hence the shear stress. The photocurrent is converted to voltage via a SR 570 current preamplifier. The photodiode transduction scheme was selected after consideration of a variety of sensing schemes which we have previously implemented.[3,5,6] This scheme yields a highly sensitive measurement which does not require integration of detection electronics and is substantially insensitive to environmental effects such as EMI and stray charging when compared with higher-impedance transduction techniques such as capacitive detection.

As previously reported, static calibrations demonstrate the linearity of this device over a shear-stress range of $0.0014\ Pa$ to $10\ Pa$ (see Figure 4).[9] This data indicates that the sensor responds linearly to within ± 1 %. In addition, the device has demonstrated minimal drifts in sensitivity.[25] Qualitative spectra from this sensor spectra indicate a bandwidth in excess of $10\ kHz$.[11] The noise floor of the sensor is $0.0004\ Pa$. The actual characteristics of the frequency response function, however, are presently unknown. Therefore, in order to use this device to obtain quantitative turbulence information the effects of the inherent mass, compliance, and dissipation of the floating-element structure on the dynamic response must be characterized. In the case of our floating-element sensor, the static calibration data and the stability of the system lead to the assumption that the micromachined shear stress sensor is a linear, time-invariant system. Therefore, the frequency response function, $H(\omega)$, can be obtained by providing the system with a known input and observing the output. In this experiment, the known shear-stress, $\tau_{St}(\omega)$, is obtained via Equation (8) and the measured shear-stress is obtained by dividing the sensor voltage, $V(\omega)$, by the static sensitivity , $\frac{\partial \overline{V}}{\partial \overline{\tau}}$ (see Figure 4),

$$H(\omega) = \frac{V(\omega)}{\tau_{St}(\omega)} \frac{\partial \overline{\tau}}{\partial \overline{V}}. \tag{14}$$

Experimental Results

Because the magnitude of the shear-stress is proportional to the product of the acoustic pressure and the square-root of the excitation frequency (see Equation (8)), it was necessary to drive the speaker at approximately 150 dB to ensure a measurable signal (*e.g.*, $> 0.0004\ Pa$) at the lower frequencies. Figure 5 shows the dynamic response of the MIT speaker/plane-wave tube system plotted versus the JBL factory specifications.[27] The response monotonically increases from $100\ Hz$ to $1\ kHz$ and then monotonically decreases with increasing frequency. The presence of a notch at $600\ Hz$ corresponds with a resonant structural mode of the acrylic tube. At resonance, a portion of the acoustic energy radiated by the speaker drives the structural vibration of the tube rather than propagating downstream. As a result, the microphone measures a lower sound pressure level. After the structural resonance,

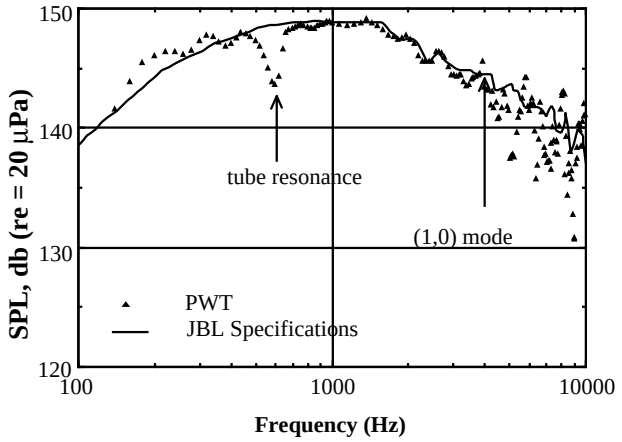

Fig. 5 Plot showing the pressure response of the plane wave tube (PWT) and the manufacturers' calibration curve for the JBL 2446J speaker driver.

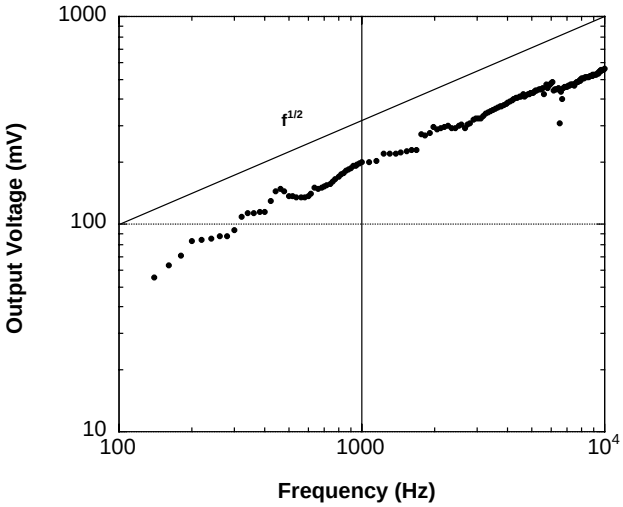

Fig. 6 Output voltage of a $500\mu m$ sensor to acoustic plane-wave excitation.

the JBL specifications and our measured results are in agreement to within $\pm 1\ dB$ up to the cut-off frequency for the (1,0) mode, $\approx 4\ kHz$. Based on this figure, the Stokes layer dynamic calibration will be valid over the frequency range 700 Hz to 4 kHz.

The shear-stress sensor output voltage for a sinusoidal pressure sweep at nominally 150 dB is shown in Figure 6. The sensor output exhibits a square-root dependence on frequency as predicted by Equation (8). It is evident that the sensor is responding to shear stress and *not pressure*, since the square-root frequency dependence dominates the variation in sound pressure level shown in Figure 5. The sensitivity of the shear-stress sensor to pressure was further tested by rotating the sensor 90° to the axial direction. The sensor displayed negligible sensitivity to acoustic forcing at 150 dB. Finally, the voltage output of the sensor

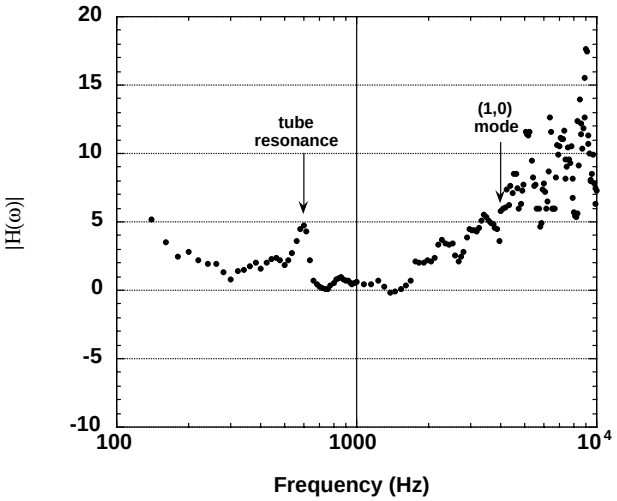

Fig. 7 A bode plot showing the magnitude of the shear-stress sensor frequency response function in dB as a function of frequency for a $500\mu m$ sensor.

displays square-root frequency well beyond the onset of the first higher-order mode. At frequencies greater than 4 kHz, the wavefront will consist of other modes in addition to the fundamental. Although, Equation (8) is invalid in this region, the sensor appears to be responding to shear-stress up to at least 10 kHz

The magnitude of the shear-stress sensor frequency response function (Equation 14) is shown in Figure 7. Ideally, the response should be 0 dB. In Figure 7, the response is between 0 dB and 5 dB over the frequency range of 700 Hz to 4 kHz. The positive shift in response is most likely due to the Stokes layer solution under-predicting the actual shear stress due to the acoustic wave. This under-prediction could be associated with tube vibration which would increase the uncertainty in modeling the problem with Equation 1. In particular, an additional term accounting for the radial wall velocity would be necessary and a compliant boundary condition would be necessary for the plane-wave eigenvalue problem (Equation 11).

Conclusions

Direct, *in-situ* dynamic calibration of a shear-stress sensor has been achieved. This technique uses plane, purely-traveling, acoustic waves to generate an oscillating shear stress. The theoretical and practical aspects of this technique are presented. A plane-wave tube apparatus was constructed and a floating-element shear-stress sensor calibrated. According to the theoretical design, the calibration indicates a nominally flat sensor response up 4 kHz, the frequency cut-off of the derived pressure-shear relationship. Based on the square-root frequency scaling of oscillating shear-stress, this sensor demonstrates a qualitative response to at least 10 kHz.

Future work in this area will focus on improving the accuracy and bandwidth of the Stokes layer calibra-

tion technique. Specifically, a smaller-area rectangular duct with better vibration isolation will be investigated. The ultimate goal is to extend this broadband technique to a variable-mean duct flow.

Acknowledgments

Support for this work was provided by the Air Force Office of Sponsored Research (Contract #: F49620-93-1-0194), and NASA (Contract #: NAG-1-1785). Samples were fabricated and packaged in the Microsystems Technology Laboratories (MTL), and the staff of the MTL are thanked for their assistance. SOI wafers for the second generation sensor fabrication were generously provided by the Motorola Semiconductor Products Sector (Direct Wafer Bonding Group). We would also like to acknowledge Sarah Lee, Mike Fedor, and Chris Protz for their assistance in obtaining the dynamic response data. Finally, the authors thank K. Uno Ingard and Richard Wlezien for their helpful technical discussions.

References

[1]Haritonidis, J.H., "The Measurement of Wall Shear Stress", Advances in Fluid Mechanics Measurements, Springer-Verlag, 1989, 229-261.

[2]Padmanabhan, A., Sheplak, M., Breuer, K.S., and Schmidt, M.A., "Micromachined sensors for static and dynamic shear-stress measurements in aerodynamic flows," Technical Digest, Transducers '97, Chicago, IL, 1997, 137-140.

[3]Schmidt, M.A., Howe, R.T., Senturia, S.D., and Haritonidis, J.H., , "Design and Calibration of a Microfabricated Floating-Element Shear-Stress Sensor", *Transactions of Electron Devices*, Vol. ED-35, pp. 750-757, 1988.

[4]Oudheusden, B. and Huijsing, J., "Integrated Flow Friction Sensor" *Sensors and Actuators A*, Vol. 15, pp. 135-144, 1988.

[5]Ng, K., "A Liquid Shear-Stress Sensor Using Wafer-Bonding Technology", *M.S. Thesis*, MIT Department of Electrical Engineering and Computer Science, 1990.

[6]Goldberg, H.D., Breuer K.S., and Schmidt, M.A., "A Silicon Wafer-Bonding Technology for Microfabricated Shear-Stress Sensors with Backside Contacts", *Technical Digest*, Solid-State Sensor and Actuator Workshop, pp. 111-115, 1994.

[7]Liu, C., Tai, Y.C., Huang, J., and Ho, C.M., "Surface Micromachined Thermal Shear Stress Sensor," *Proceedings, The ASME Symposium on Application of Microfabrication to Fluid Mechanics*, ASME Winter Annual Meeting, Chicago, 1994.

[8]Jiang, F., Tai, Y.C., Ho, C.M., and Li, W.J., "A Micromachined Polysilicon Hot-Wire Anemometer" *Technical Digest, Solid-state Sensor and Actuator Workshop, Hilton Head Island*, pp. 264-267, 1994.

[9]Padmanabhan, A., Goldberg, H.D., Schmidt, M.A., and K.S. Breuer, "A Wafer-Bonded Floating-Element Shear-Stress Microsensor with Optical Position Sensing by Photodiodes", *IEEE J. MEMS*, Vol. 5, No. 4, pp. 307-315, 1996.

[10]Pan, T., Hyman, D., Mehregany, M., Reshotko, E., and Williams, B., "Characterization of microfabricated shear stress sensors," *Proceedings of 16th International Congress on Instrumentation in Aerospace Simulation Facilities*, WPAFB, OH, July 1995.

[11]Padmanabhan, A., Goldberg, H.D., Schmidt, M.A., and Breuer, K.S., "A Silicon Micromachined Sensor for Shear Stress Measurements in Aerodynamic Flows", *AIAA Paper 96-0422*, January 1996.

[12]Kälvesten, E., "Pressure and Wall Shear Stress Sensors for Turbulence Measurements", *Ph.D. Thesis*, Royal Institute of Technology, Stockholm, Sweden, 1996.

[13]Jiang, F., Tai, Y.C., Gupta, B., Goodman, R. Tung, S, Huang, J.B., and Ho, C.M., "A Surface-Micromachined Shear Stress Imager," *Proc. IEEE Micro-electromechanical Systems (MEMS '96)*, San Diego, pp. 110-115, 1996.

[14]Bellhouse, B.J. and Schultz, D.L., "The Determination of Fluctuating Velocity in Air with Thin Film Gauges," *J. of Fluid Mech.* Vol. 29, No. 2, pp. 289-295, 1967.

[15]Brison, J.F., Charnay, G., and Comte-Bellot, G., "Calculation of the Heat Transfer Between a Hot Film and a Substrate Using a Two-Dimensional Model: Prediction of the Dynamic Response for Ordinary Probes," *Int. J. Heat Mass Transfer*, Vol. 22, No. 1, pp. 111-119, 1979.

[16]Perry, A.E., Smits, A.J., and Chong, M.S., "The Effects of Certain Low Frequency Phenomena on the Calibration of Hot Wires," *J. of Fluid Mech.*, Vol. 90, pp. 415-431, 1979.

[17]Glauser, M.N., *private communication* about Arizona State University's Sensor Fest '97 1998.

[18]White, F.M., *Viscous Fluid Flow*, McGraw-Hill, New York, pp. 143-148, 1974.

[19]Oppenheim, A.V., Willsky, A.S., and Young, I.T, *Signals and Systems*, Prentice-Hall, Englewood Cliffs, New Jersey, Chapt. 3, 1983.

[20]Bendat, J.S. and Piersol, A.G., *Engineering Applications of Correlation and Spectral Analysis*, Wiley-Interscience, Chapt. 5, New York, 1993.

[21]Richardson, E.G., and Tyler, E., "The Transverse Velocity Gradients Near Mouths of Pipes in Which an Alternating or Continuous Flow of Air is Established," *Proc. Phys. Soc. Lond.*, Vol. 42, pp. 1-15, 1929.

[22]Sexl, T. *Z. Phys.,* "Über die von E.G. Richardson entdeckten Annulareffekt," Vol. 61, pp. 349-362, 1930.

[23]Abramowitz, M. and Stegun, I.A. *Handbook of Mathematical Functions*, 9^{th} ed., Dover, New York, 1972.

[24]Morse, P.M. and Ingard, K.U., *Theoretical Acoustics*, McGraw-Hill, New York, chap. 9, 1968.

[25]Padmanabhan, A., "Silicon Micromachineds Sensors and Sensor Arrays for Shear Stress Measurements in Aerodynamic Flows", *Ph.D. Thesis*, MIT Department of Mechanical Engineering, 1997.

[26]Freymuth, P., "Calculation of Square Wave Test for Frequency Optimised Hot-Film Anemometers," *J. Phys. E: Sci. Instrum.*, Vol. 14, pp. 238-240, 1981.

[27]JBL Professional, 2446H/J Compression Driver Specification Sheet, Northridge, California.